The Journal of Korean Vacuum Science & Technology
Vol. 2, No. 2, October 1998, pp. 78~84

Properties of ZnO:Al thin films prepared by a single target sputtering

Ilsin An, Chang-Hyo Lee, You-Shin Ahn, and Won-Taeg Lim

Department of Physics and Research Center for Electronic Materials and Components
Hanyang University, Ansan 425-791 Korea
(Received June 18, 1998)

Abstract – ZnO:Al films were prepared by an rf magnetron sputtering and targets for the experiments were fabricated by sintering the mixture of ZnO and Al_2O_3. The most conductive film was obtained from the target with 2.0~2.2 wt.% of Al_2O_3. Optical properties studied with spectroscopic ellipsometry showed bandgap widening, i.e., the Burstein-Moss shift, with aluminum doping as well as with the elevation of deposition temperature. And it is found that the optical and electrical properties were related to the density of states as well as the variation of donor level. When hydrogen atoms were introduced into the films, the activation energy for the generation of oxygen vacancy was smaller for the films showing higher conductivity. This indicates that the optimum deposition condition for highly conductive ZnO:Al film has strong relation to the optimum doping condition.

I. Introduction

Zinc oxide (ZnO) thin films show interesting electrical, optical, and mechanical properties. Thus, they have potential applications in various optoelectronic devices such as conducting windows [1], surface acoustic wave devices [2], and gas sensors [3]. Besides the lower cost of material, ZnO shows better stability over indium or tin-based oxides in hydrogen ambient [4]. For example, when solar cells or electroluminescence devices are fabricated, transparent conducting oxides such as indium tin oxide (ITO) or SnO_2 are used as substrate materials and hydrogen plasma processes are commonly followed. Thus, when the amorphous silicon based films are deposited onto these substrates using silane gas, hydrogens are produced in the plasma. These hydrogen species are known to reduce ITO or SnO_2 into elemental metal species [5, 6]. Although ZnO films show better stability, they exhibit slight optical gap widening upon hydrogen incorporation [7].

ZnO is a wide band gap material which provides high transparency in the visible spectrum and this is useful for solar cell application. Besides, the optical and electrical properties of ZnO can be easily tailored by doping with various foreign elements such as Cu, Cr, B, Ga, Al, etc [8-11]. Among them, aluminum doped ZnO (ZnO:Al) has been widely studied for its possible application to a transparent conducting material in place of costing ITO [12-17].

In this study, we present the optical and electrical properties of ZnO:Al films in conjunction with hydrogenation.

II. Experimental Details

High purity ZnO powder was calcined at 1100°C for three hours and mixed with Al_2O_3 powder in a proper weight ratio. This mixture was milled and poured into cylindrical hollow mold of two inches in diameter. After pressing under a cold and dry condition the final disk was sintered at 1200°C for 9 hours in the electric furnace to produce ⅛ inch-thick ZnO:Al target. We

often observed 4~5% reduction in diameter in the sintering process.

ZnO:Al films were fabricated by conventional magnetron rf sputtering with a two-inch single target system. The doping level of Al_2O_3 (C_{Al}) was varied from 0 to 2.4 wt.%. These values were close to the actual aluminum contents in the grown films from energy dispersion spectroscopy measurements. Argon was used as a working gas and pressure was maintained at 5 mTorr during deposition. An rf power was fixed at 60 W and pre-sputtering was performed for 5 minutes in each deposition. And substrate temperature (T_S) was varied from 25°C to 300°C. For ellipsometric measurements, crystalline silicon wafer was used as a substrate with ~20 Å native oxide intact. Also Corning glass was used for electrical measurements.

In hydrogenation experiment, atomic hydrogen was produced by a hot filament method [7]. In this method, atomic hydrogens were generated by igniting tungsten filament in 300 mTorr hydrogen ambient. For optical studies, we employed spectroscopic ellipsometry whose spectral range lies between 1.5 and 5.0 eV. The surface morphology of ZnO(:Al) films was studied by scanning tunneling microscopy (STM). Also X-ray diffraction, scanning electron microscopy, and electrical measurements were performed.

III. Results and Discussion

A. Electrical and optical properties

The optical properties of ZnO:Al films were obtained from spectroscopic ellipsometry measurements. Ellipsometric spectra {$\Delta(h\nu)$, $\psi(h\nu)$} were inverted into {$\varepsilon_1(h\nu)$, $\varepsilon_2(h\nu)$} spectra under the assumption of single layer model for ZnO:Al films, where ε_1 and ε_2 are the real and imaginary part of complex dielectric function and they are functions of photon energy. The assumption of single-layered film was appropriate from the cross sectional view of scanning electron micrograph. In order to avoid the thickness-dependence in the electrical and optical properties, the thickness of each film was kept ~1000 Å for reliable comparison.

The dielectric functions for undoped ZnO and 1.6~2.4 wt.% of Al_2O_3 doped ZnO:Al films were presented in Fig. 1. Deposition temperature for the films was 250°C. Two distinct features appeared upon doping. First, the abrupt peaks near absorption edge in undoped ZnO diminished with aluminum doping. This might be related to the loss of some crystallinity upon doping. Second, the optical gap, E_{op}, (i.e., the onset of ε_2 rise around 3.3 eV) shifted toward higher energy upon doping. This is the Burstein-Moss (BM) effect caused by filling of narrow conduction band [18]. The shift of the optical gap by the BM effect, ΔE, can be written as

$$E_{op} = E_g + \Delta E \quad (1)$$

where E_g is an intrinsic gap. And the BM shift can be expressed as following

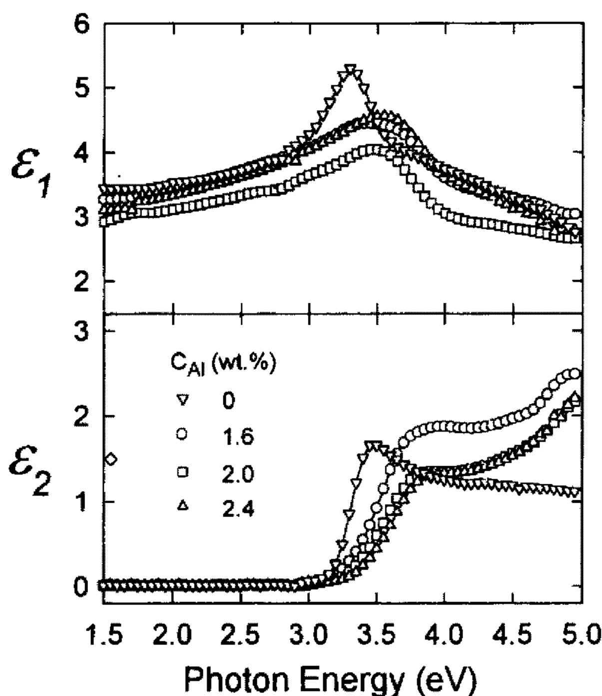

Fig. 1. Dielectric functions of ZnO:Al thin films prepared at different C_{Al} (T_s=250°C).

$$\Delta E = h^2 N^{2/3}/(8m^* \pi^{2/3}) \tag{2}$$

where h is the Planck constant, N is the carrier density, and m* is an effective mass of carrier.

The absorption coefficient α near an absorption edge can be given by

$$\alpha(h\nu) = (h\nu - E_{op})^{1/2} \tag{3}$$

where hν is the photon energy. Thus, the optical gap, E_{op} can be estimated from the linear extrapolation of the squares of the absorption coefficients versus the photon energy near 3.3 eV [13, 19]. The absorption coefficients can be calculated from the dielectric functions such as shown in Fig. 1. E_{op}'s are shown for ZnO:Al films with different C_{Al} in Fig. 2, where E_{op} was increased from 3.27 to 3.48 eV with C_{Al} varying from 0 to 2.0 wt.%. Introducing the conduction-band effective mass m*=0.35 of the free electron mass [20] into Eq. (2), we can estimate the change in carrier density, $N=7.9\times10^{19}cm^{-3}$ at C_{Al} =2.0 wt.%. This result agrees with that reported in literature [12].

In Fig. 3, the resistivities of ZnO:Al films with different C_{Al} are plotted for different sets of experiments. The initial decrease in resistivity supports the blue shift of E_{op}, that is, the increase in carrier concentration upon doping as expressed

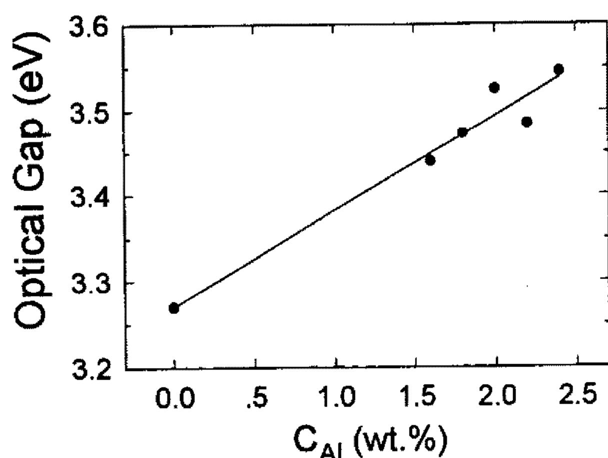

Fig. 2. Optical gaps for the samples with different C_{Al}. Optical gaps were deduced from the dielectric functions shown in Fig. 1. Line is a guide to the eye.

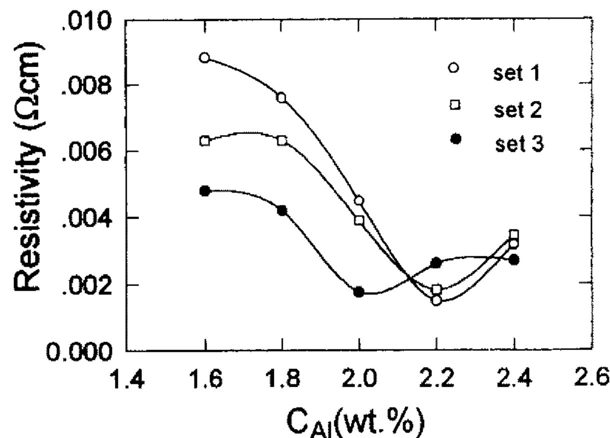

Fig. 3. Resistivity vs C_{Al} for the different sets of samples. Lines are guides to the eye.

in Eq. (2). Although we tried to keep other experimental conditions constant, the C_{Al} for lowest resistivity varied around 2.0~2.2 wt.% for different set of experiments. However, this feature was obtained consistently in the repeated experiments and similar results were reported in literature, in which ZnO:Al films were prepared by an electrodeless chemical process [13]. In this report, the rise of resistivity at high aluminum concentration was ascribed to the decrease in mobility caused by the scattering at grain boundaries. Our STM studies also showed that the grains got finer with higher C_{Al}. Although we kept film thickness around 1000 Å for better ellipsometric and structural studies, thicker films (> 3000 Å) showed one order lower resistivities.

For further investigation, we measured the resistivity versus temperature in vacuum for the samples shown in Fig. 3 (set 2). From the low temperature region of the Arrhenius plots of normalized resistance (top of Fig. 4), the donor level, E_d, versus C_{Al} could be obtained (open circles on the bottom of Fig. 4). That is, the resistivity ρ can be expressed as following [21].

$$\rho = \rho_0 \exp\{E_d/(2k_B T)\} \tag{4}$$

where k_B is the Boltzmann constant and T is an absolute temperature. ρ_0 is slightly temperature-dependent but usually regarded as a constant.

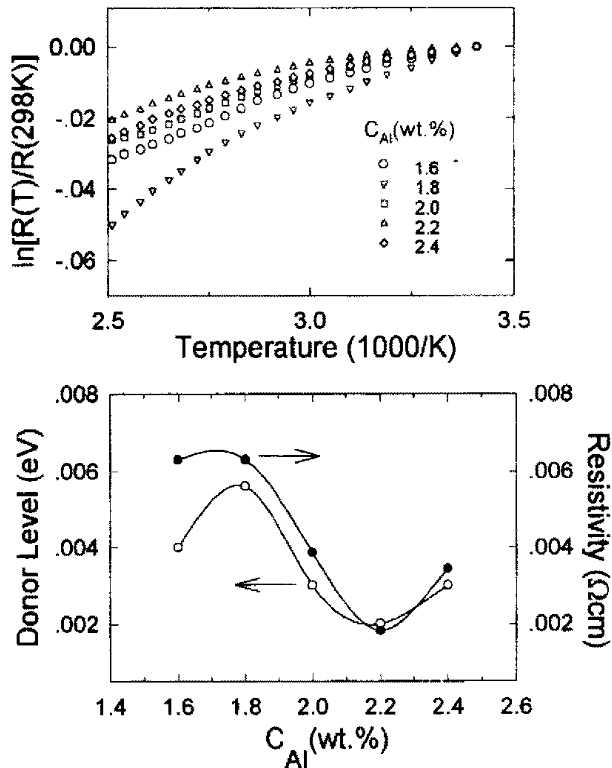

Fig. 4. (top) the Arrhenius plots of normalized resistance for the samples with different C_{Al}. (bottom) donor levels obtained from above figures (open circles) and the resistivity vs C_{Al} from the set 2 in Fig. 3 (filled circles).

Although the magnitude is small, the trend of E_d in Fig. 4 resembles that of the resistivity (see set 2 in Fig. 3). This indicates that the increase of carrier density in ZnO:Al upon aluminum doping can be achieved not only by the increase in density of states in donor level but also by the lift of donor level.

In order to investigate the effect of T_S, we varied T_S from 25°C to 300°C with a fixed value of C_{Al} at 2.0 wt.%. Fig. 5 and 6 show the dielectric functions and E_{op}'s of ZnO:Al grown at different T_S. As we can notice from both figures, E_{op} increased with T_S indicating the BM-effect. This means that the doping could be enhanced for the film grown at high T_S. Corresponding electrical properties are shown in Fig. 7, which also support the results in Fig. 6 and thus Eq. (2). In repeated experiments, we found that resistivity reached minimum when T_S exceeded ~200°C.

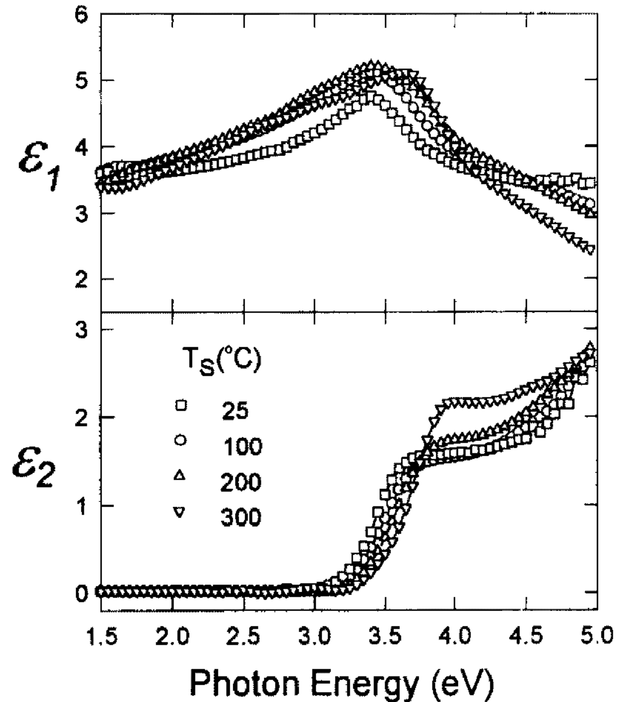

Fig. 5. Dielectric functions of ZnO:Al thin films prepared at different T_s (C_{Al}=2.0 wt.%).

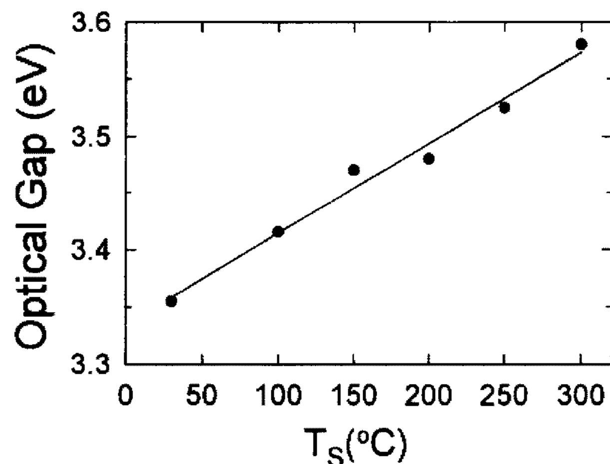

Fig. 6. Optical gaps for the samples prepared at different T_S. Optical gaps were deduced from the dielectric functions shown in Fig. 5. Line is a guide to the eye.

B. Structural properties

The optical and electrical properties of ZnO:Al films were apparently related to the morphology of the films. We performed STM studies for all sets of samples but representative figures are presented in Fig. 8 for clarity. Obviously, ZnO film without aluminum doping did not show any image due to poor conductivity. Line shaped

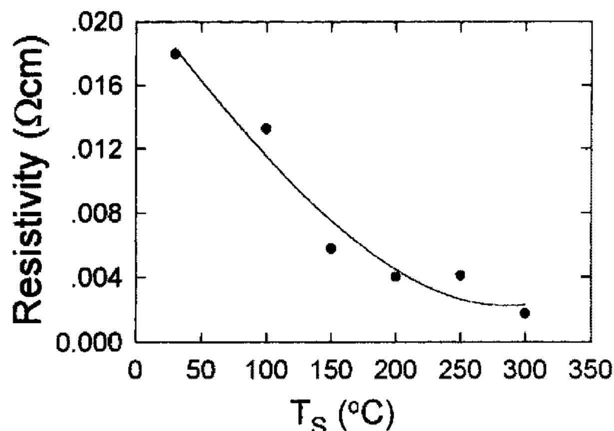

Fig. 7. Resistivity vs T_S. Line is a guide to the eye.

images in the figures are related to the growth direction of ZnO:Al. From the comparison between top and middle figures, we find that ZnO:Al with $C_{Al}=2.4$ wt.% shows finer structure than the one with $C_{Al}=2.0$ wt.%. As we mentioned earlier, smaller grains have more surface area resulting in more carrier scattering, which in turn drops the mobility and increases the resistivity of the film. The increase in content of various metals in ZnO film is known to decrease the grain size in the film [9, 12, 13]. Thus, the grain growth in the ZnO:Al was suppressed by the addition of aluminum.

The effect of T_S, can be found from the comparison of the middle and bottom figures in Fig. 8. We believe the coalescence process reduces surface area in clusters and this in turn changes the optoelectronic properties of ZnO:Al film. ZnO:Al film grown at T_S=100°C shows smaller grains and do not show clear coalesced images when compared to the one grown at T_S=250°C. This is a general trend in thin film processing. Although less carrier scattering is expected for the films grown relatively higher T_S from this microstructural analysis, the result in Figs. 6 indicated that there was also the increase in carrier density at higher T_S. Further information can be found from the following hydrogenation studies.

C. Hydrogenation

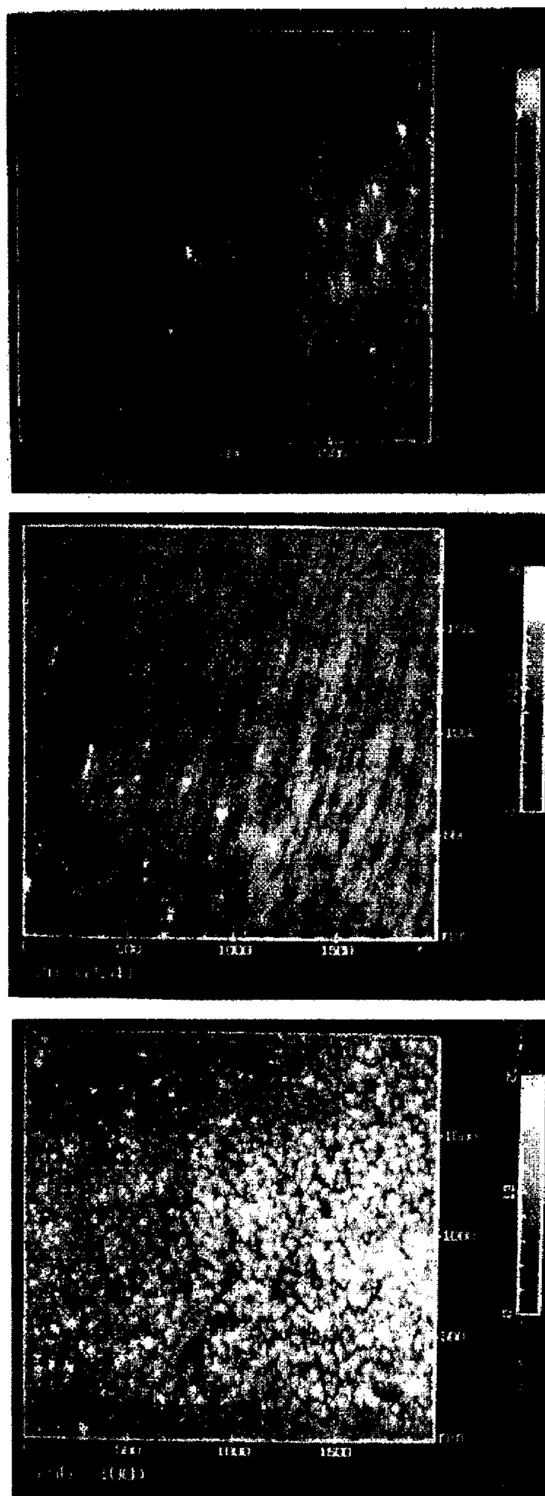

Fig. 8. STM images of ZnO:Al. (top) C_{Al}=2.0 wt.%, T_s= 250°C (middle) C_{Al}=2.4 wt.%, T_s=250°C (bottom) C_{Al}=2.0 wt.%, T_s=100°C.

Hydrogen doping improves the conductivity of ZnO:Al showing the BM effect. This phenomenon occurs through the generation of oxygen vacancies [22]. In order to derive the activation energy for

the process, ZnO:Al film was exposed to the atomic hydrogens and resistivity was measured by varying temperature. In this experiment, each measurement was taken in real time to ensure full hydrogen diffusion into the film and the resistivity near the saturation point was taken for the analysis. Although earlier work with secondary ion mass spectrometry showed easy penetration of hydrogen deep into ZnO:(Al) film with hot filament method, our analysis for the low hydrogenation temperature regime may have some uncertainties caused by diffusion-limited process.

Fig. 9 (top) shows the Arrhenius plots of the normalized resistances for the ZnO:Al films with different C_{Al} (used set 3 in Fig. 3). From the fit of linear region we can deduce the activation energy, E_a, for each sample (bottom of Fig. 9). We can use Eq. 4 by setting $E_a=\frac{1}{2}E_d$ but with different physical meaning [21, 22]. In the derivation of E_a the pure temperature effect can be safely neglected from the comparison between the top figures in Fig. 4 and Fig. 9. Both measurements during hydrogenation and dehydrogenation resulted in close E_a values and trend. This means that the oxygen vacancy generation is a reversible process. Interestingly, the trend resembles that of the resistivity vs C_{Al} (compare with set 3 in Fig. 3). When this experiment was performed on the samples grown at different T_S (used samples shown in Figs. 5~7), similar results were obtained. That is, the feature

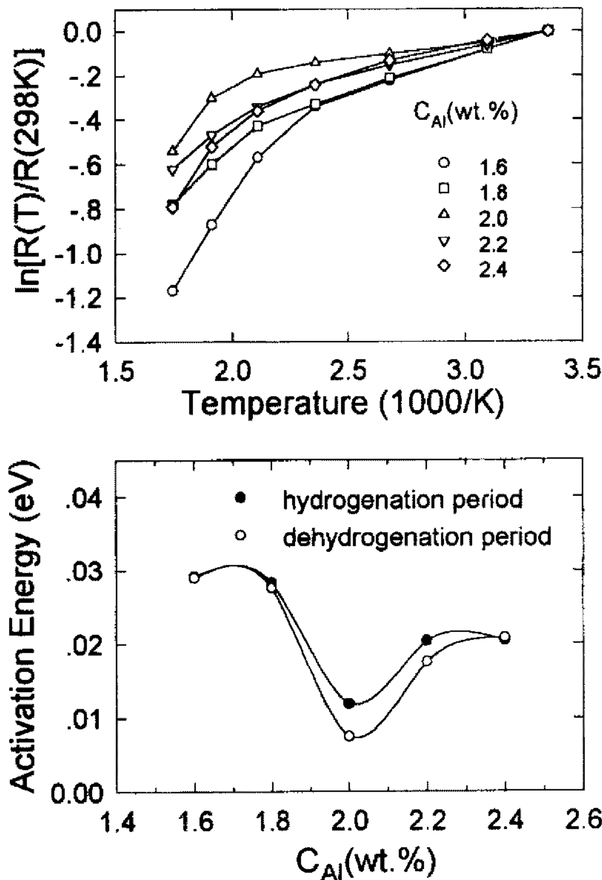

Fig. 9. (top): The Arrhenius plots of normalized resistance for the samples with different C_{Al} (used samples in sets 3 in Fig. 3). The temperature for the measurements of resistance is same as hydrogenation. (bottom): The activation energies obtained from above figures during hydrogenation (filled circles) and dehydrogenation (open circles).

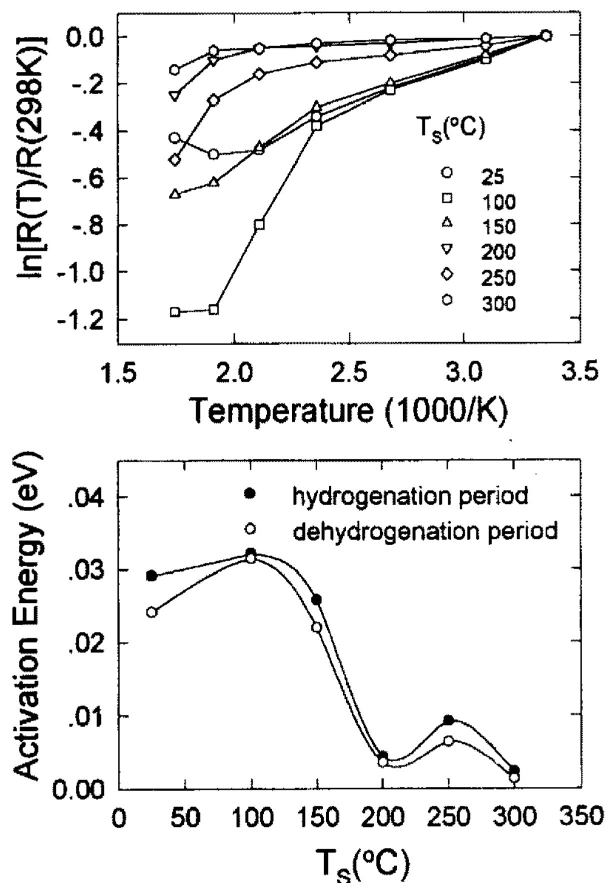

Fig. 10. (top): The Arrhenius plots of normalized resistance for the samples with different T_S. The temperature for the measurement of the resistance is same as the hydrogenation. (bottom): The activation energies obtained from above figures during hydrogenation (filled circles) and dehydrogenation (open circles).

in the bottom of Fig. 10 also resembles that in Fig. 7.

From the series of hydrogenation studies on both sets of samples, it is found that more conductive film shows smaller activation energy for the generation of oxygen vacancies.

IV. Conclusion

We investigated ZnO:Al films prepared under different substrate temperature and aluminum contents. The addition of aluminum as well as the elevation of substrate temperature increased the conductivity and widened the optical gap meaning the Burstein Moss effect. From the temperature dependence of resistivity with aluminum doping, we found that the increase in donor level also contributed to the BM effect besides the increase in density of states. When hydrogenation studies were performed on each sample, more conductive sample showed smaller activation energy for the process. Thus, we can conclude that the optimum deposition condition for highly conductive ZnO:Al film is at least related to the condition for the generation of oxygen vacancies.

Acknowledgment

This work was supported by Korea Science and Engineering Foundation (951-0209-039-2).

References

1. Y. Matsumoto, G. A. Hirata, H. Takakura, H. Okamoto, and Y. Hamakawa, J. Appl. Phys. **67**, 6538 (1990).
2. F. S. Hickernell, IEEE Trans. Sonics Ultrason. **SU-32**, 621 (1980).
3. U. Lampe and J. Muller, Sensors Actuators **18**, 269 (1989).
4. S. Kumar and B. Drevillon, J. Appl. Phys. **65**, 3023 (1989).
5. S. Major, S. Kumar, M. Bhatnagar, and K. L. Chopra, Appl. Phys. Lett. **49**, 394 (1986).
6. J. H. Thomas III, Appl. Phys. Lett. **42**, 794 (1983).
7. I. An, Y. Lu, C. R. Wronski, and R. W. Collins, Appl. Phys. Lett. **64**, 3317 (1994).
8. K. Kobayashi, H. Udaka, S. Matsushima, and G. Okada, Jpn. J. Appl. Phys. **32**, 3854 (1993).
9. M. Shinoda, T. Nishida, Y. Sawada, M. Hosaka, and T. Matsumoto, Jpn, J. Appl. Phys. **32**, L1565 (1993).
10. W. W. Wenas, A. Yamada, K. Takahashi, M. Yoshino, and M. Konagai, J. Appl. Phys. **70**, 7119 (1991).
11. S. Kohini, M. Nishitani, and T. Wada, J. Appl. Phys. **75**, 2069 (1994).
12. Z. -C. Jin, I. Hamberg, and C. G. Granqvist, J. Appl. Phys. **64**, 5117 (1988).
13. Raviendra D. and J. K. Sharma, J. Appl. Phys. **58**, 838 (1985).
14. Y. Igasaki and H. Saito, J. Appl. Phys. **69**, 2190 (1991).
15. J. Hu and R. G. Gordon, J. Appl. Phys. **71**, 880 (1992).
16. B. E. Sernelius, K.-F. Berggren, Z.-C. Jin, I. Hamberg, and C. G. Granqvist, Phys. Rev. **B37**, 10244 (1988).
17. K. Yamaya, Y. Yamaki, H. Nakanishi, and S. Chichibu, Appl. Phys. Lett, **72**, 235 (1998).
18. E. Burstein, Phys. Rev. **93**, 632 (1954).
19. F. Quaranta, A. Valentini, F. R. Rizzi, and G. Casamassima, J. Appl. Phys. **74**, 244 (1993).
20. A. Sarkar, S. Ghosh, S. Chaudhuri, and A. K. Pal, Thin Solid Films **204**, 255 (1991).
21. Y. Natsume, H. Sakata, T. Hirayama, and H. Yanagida, J. Appl. Phys. **72**, 4203 (1992).
22. T. Minami, H. Nanto, S. Shooji, and S. Takata, Thin Solid Films **111**, 167 (1984).